

# **Mo-Si-B Alloy Development**

## **J. H. Schneibel**

Oak Ridge National Laboratory, Metals and Ceramics Division, P. O. Box 2008, Oak Ridge, TN 37831-6115

E-mail: [schneibeljh@ornl.gov](mailto:schneibeljh@ornl.gov); Telephone: (865) 576-4644; Fax: (865) 574-7659

## **Jamie J. Kruzic**

Lawrence Berkeley National Laboratory, 1 Cyclotron Road, Berkeley, CA 94720, U.S.A.

Email: [jjkruzic@lbl.gov](mailto:jjkruzic@lbl.gov); Telephone: (510) 486-5544; Fax: (510) 486-4995

## **Robert O. Ritchie**

Lawrence Berkeley National Laboratory, 1 Cyclotron Road, Berkeley, CA 94720, U.S.A.

Email: [roritchie@lbl.gov](mailto:roritchie@lbl.gov); Telephone: (510) 486-5798; Fax: (510) 486-4881

## **INTRODUCTION**

In order to increase the thermodynamic efficiency of fossil energy systems, strong, tough and oxidation resistant materials capable of service temperatures well beyond 1000°C are needed. While refractory elements such as Nb, Mo, Ta, and W have high melting points, they lack oxidation resistance. Refractory element silicides, on the other hand, can be oxidation resistant. For example, MoSi<sub>2</sub> is widely used in heating elements for resistance furnaces. Its good oxidation resistance is due to the formation of a protective silica glass scale. However, MoSi<sub>2</sub> is very brittle with a room temperature fracture toughness on the order of 3 MPa m<sup>1/2</sup>.<sup>1</sup> Also, it is very weak at high temperatures<sup>1</sup>. Berczik<sup>2,3</sup> has pioneered alloys consisting of Mo<sub>3</sub>Si, Mo<sub>5</sub>SiB<sub>2</sub> (“T2”), and a toughening Mo solid solution ( -Mo). The boron in these alloys improves their oxidation resistance. This is because boron reduces the viscosity of the glassy silica scale that forms on these alloys during exposure to air.<sup>4,5</sup> The low viscosity helps to maintain a continuous protective oxide scale. Since these alloys contain a ductile phase, -Mo, they can exhibit respectable fracture toughness values. For an -Mo volume fraction of 49%, room temperature initiation and peak toughness values of, respectively, 12 and 21 MPa m<sup>1/2</sup> have been reported.<sup>6</sup> While the fracture toughness increases as the -Mo volume fraction increases, the oxidation resistance decreases. The optimization of Mo-Mo<sub>3</sub>Si-T2 alloys requires therefore a trade-off between fracture toughness on the one hand, and oxidation resistance on the other. This paper compiles data illustrating the opposite trends in the fracture toughness and oxidation resistance as the -Mo volume fraction increases. In order to have a sufficiently high volume fraction of toughening -Mo, oxidation-resistant coatings are being considered. Preliminary experiments assessing the thermal expansion mismatch and the thermodynamic compatibility of potential coatings for Mo-Si-B silicides are presented. Another approach aims at improving the toughening efficiency of the -Mo phase (thus reducing the volume fraction required to achieve adequate toughness) by making it more ductile. Microalloying with Zr is shown to be successful in this regard. Scruggs showed that the room temperature ductility of Mo increases, when MgAl<sub>2</sub>O<sub>4</sub> or NiAl<sub>2</sub>O<sub>4</sub> spinel particles are added.<sup>7</sup> However, our experimental results on the Scruggs effect are so far inconclusive.

## **DISCUSSION OF CURRENT ACTIVITIES**

### **Experimental Procedures**

The alloys in this work were prepared by arc-melting elemental starting materials in a partial pressure of argon (70 kPa) on a water-cooled copper hearth. The purity of the starting materials Mo, Si, Zr and B was 99.95, 99.99, 99.5, and 99.5 weight % (wt%), respectively. Unless stated otherwise, alloy compositions will be in atomic % (at. %). The alloys were re-melted several times in order to improve their homogeneity. Some alloys were drop-cast into cylindrical water-cooled copper molds with diameters of 12.5 or 25 mm. Alloys containing Al or Mn experienced significant weight losses during arc-melting due to evaporation. Their composition after casting was re-calculated assuming that the weight loss was exclusively due to losses in Al or Mn, respectively.

Metallography specimens were prepared by grinding, mechanical polishing, and etching in Murakami’s reagent. Microstructural examination was carried out by optical microscopy as well as scanning electron microscopy (SEM). The phases were identified by a combination of energy dispersive spectroscopy (EDS) in an SEM, by wavelength-dispersive spectroscopy (microprobe), and powder x-ray diffraction.

Thermal expansion measurements were carried out with 25 mm long specimens in argon in a Theta Industries Inc. dilatometer.

Mo powders (2-8  $\mu\text{m}$ ) with and without  $\text{MgAl}_2\text{O}_4$  spinel particles (-325 mesh,  $<45 \mu\text{m}$ ) were hot-pressed in graphite dies *in vacuo* (rotary pump) for times ranging from 1 to 4 hours at  $1800^\circ\text{C}$  and a pressure of 21 MPa. Tensile test specimens were cut by electro-discharge machining and finished with 600 grit SiC paper prior to testing.

For the purpose of screening tests, the fracture toughness  $K_{\text{q}}$  was determined from flexure tests with chevron-notched flexure bars<sup>8</sup> with a cross-section of  $3 \times 4 \text{ mm}$  and a span of 20 mm (see also Fig. 1):

$$K_{\text{q}} = [EG/(1 - \nu^2)]^{1/2}, \quad (1)$$

where  $E$  is Young's modulus,  $G = W/A$  is the work  $W$  expended during fracture divided by the area  $A$  swept out by the crack, and  $\nu$  = Poisson's ratio. The fracture toughness values determined with this technique tend to be higher than those determined with more rigorous techniques. On the other hand, this technique requires less sample material, is simpler to implement than more rigorous techniques, and is considered suitable for comparative purposes.

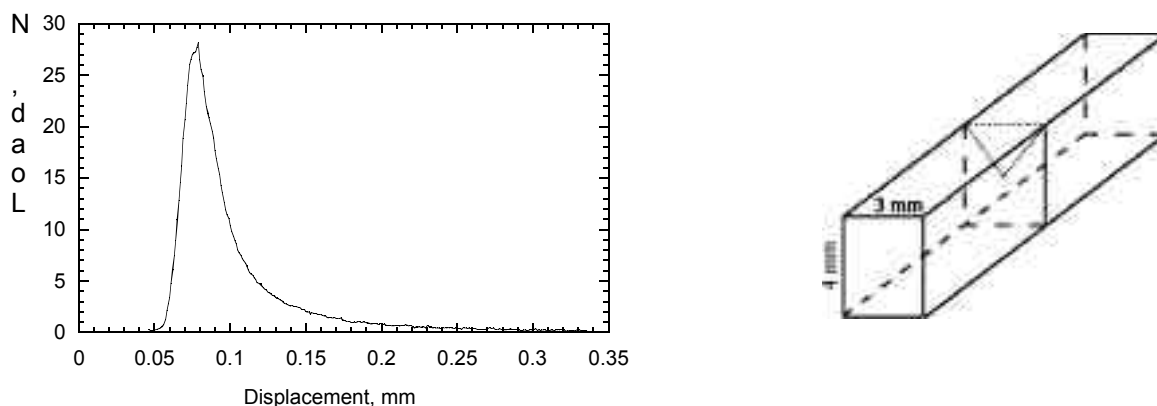


Figure 1. Determination of  $K_{\text{q}}$  from flexure tests with chevron-notched flexure bars

For some specimens, precise fracture toughness values were obtained under plane-strain conditions by monotonically loading fatigue-precracked, disk-shaped compact-tension DC(T) specimens to failure.<sup>6,9</sup> During these tests, crack lengths were periodically monitored using the elastic unloading compliance. Following pre-cracking, specimens were cycled for 24 hr at the  $K_{\text{TH}}$  threshold (where there is no discernable crack growth) in an attempt to remove any possible crack bridging in the wake of the pre-crack. The resistance curve ( $R$ -curve) behavior was then evaluated by measuring the crack-growth resistance,  $K_{\text{R}}$ , as a function of crack extension,  $a$ .

### Fracture Toughness and Oxidation Resistance vs. $\alpha$ -Mo Volume Fraction

Figures 2 and 3 summarize oxidation and fracture toughness data for Mo-Si-B alloys.<sup>10-12</sup> The oxidation data include the large initial mass loss due to evaporation of  $\text{MoO}_3$ . A more thorough comparison would have to compare the oxidation rates following the initial mass loss. The fracture toughness of pure Mo was approximated by the value for a Mo-1Zr alloy.<sup>13</sup> Rigorously measured data for Mo-Si-B containing 49 vol.% of continuous  $\alpha$ -Mo phase are shown as well.<sup>6</sup> The two figures show that oxidation resistance and fracture toughness depend in opposite ways on the  $\alpha$ -Mo volume fraction. As the  $\alpha$ -Mo volume fraction increases the fracture toughness increases, whereas the oxidation resistance decreases. Oxidation resistant coatings could be one potential solution to this dilemma. Another potential solution is to improve the toughening effectiveness of the Mo phase, i.e., make it more ductile. Then less  $\alpha$ -Mo would be required in order to reach the desired fracture toughness. This, in turn, would result in an improvement of the oxidation resistance. The ductilization approach is realistic since the room temperature fracture surface of a high-toughness silicide alloy (that shown by the diamonds in Fig. 3 [ref. 6]) indicates a significant fraction of intergranular fracture in the  $\alpha$ -Mo phase (Fig. 4). If intergranular fracture can be inhibited, an even higher fracture toughness is likely. In this work, two ductilization

approaches will be assessed. One of them involves microalloying with Zr, and the other the addition of spinel particles to the Mo phase.

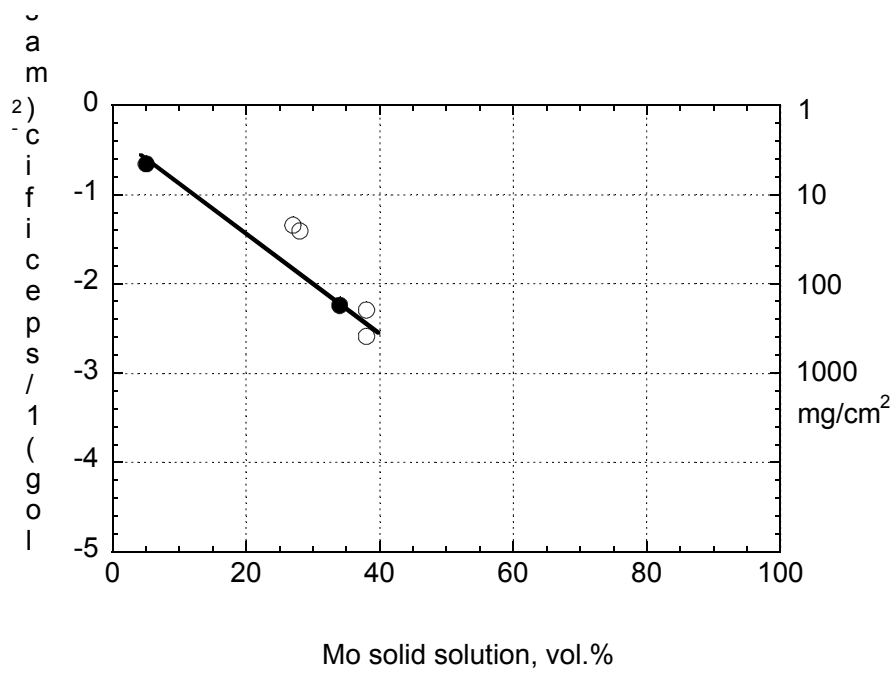


Fig. 2. Specific mass loss for Mo-Si-B alloys after oxidation for durations from 20 and 24 hours at 1200°C, as a function of the  $\gamma$ -Mo volume fraction. The full circles correspond to specimens containing individual  $\gamma$ -Mo particles, and the white circles to specimens containing continuous  $\gamma$ -Mo.

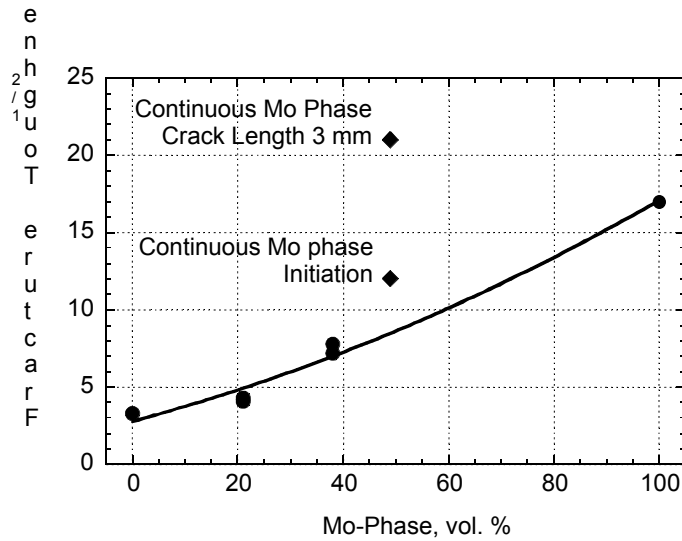


Fig. 3. Room temperature fracture toughness of Mo-Si-B alloys as a function of the  $\gamma$ -Mo volume fraction. The values for the Mo-1 wt% Zr alloy (“100% Mo-Phase”) and the silicide with 49 vol.% of a continuous  $\gamma$ -Mo phase (diamonds) were obtained with rigorous testing techniques. The values for 49 vol.%  $\gamma$ -Mo illustrate the extent by which the fracture toughness can be increased if the  $\gamma$ -Mo is coarse and continuously distributed.

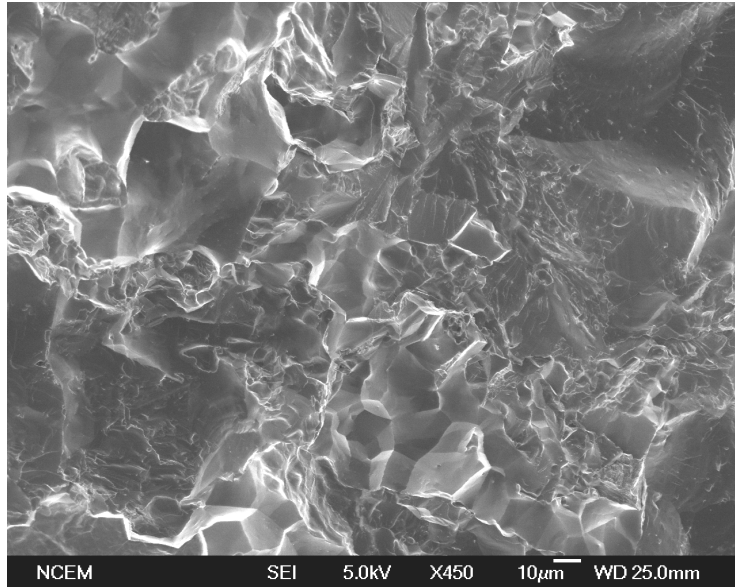


Fig. 4. SEM micrograph of fracture surface of Mo-Si-B specimen containing 49 vol.% of continuous  $\beta$ -Mo phase. Most of the flat cleavage facets correspond to fracture of the intermetallic phases. The  $\beta$ -Mo phase exhibits a significant fraction of intergranular fracture.

### Coatings

Fig. 5 compares the thermal expansion of  $\text{Al}_2\text{O}_3$  to that of Mo,  $\text{Mo}_3\text{Si}$ , and  $\text{Mo}_5\text{SiB}_2$ .<sup>14,15</sup> Since  $\text{Al}_2\text{O}_3$  has a higher expansion coefficient than the silicide phases, it is not suitable as a coating. This is because upon cooling, tensile stresses would be set up in the  $\text{Al}_2\text{O}_3$  and cracking would presumably occur. If the thermal expansion coefficient of the silicide could be increased, a better match with that of  $\text{Al}_2\text{O}_3$  would result. Figure 6 shows the thermal expansion of Mo-12Si-8.5B (at. %). Alloying with Al increased the thermal expansion slightly, whereas alloying with Mn reduced it. These results suggest that it would be difficult to increase the CTE of Mo-Si-B alloys to match that of  $\text{Al}_2\text{O}_3$ . Coatings other than  $\text{Al}_2\text{O}_3$ , with lower thermal expansion, may be a more realistic option. Figure 7 compares the thermal expansion of calcium aluminate,  $\text{CaAl}_4\text{O}_7$ , hafnium silicate  $\text{HfSiO}_4$ , and mullite,  $3\text{Al}_2\text{O}_3 \cdot 2\text{SiO}_2$  (ref. 16) with that of Mo-12Si-8.5B. Since these coating materials have a lower CTE than Mo-12Si-8.5B, they are less likely to spall during cyclic oxidation. However, x-ray diffraction of a  $\text{CaAl}_4\text{O}_7$  coating applied to Mo-12Si-8.5B showed the phases Mo,  $\text{Al}_2\text{O}_3$ , and  $\text{CaAl}_2\text{Si}_2\text{O}_8$  (calcium aluminosilicate, also called anorthite) indicating that this coating is not thermodynamically stable in contact with molybdenum silicides. The thermodynamic stability of mullite is presently under investigation.

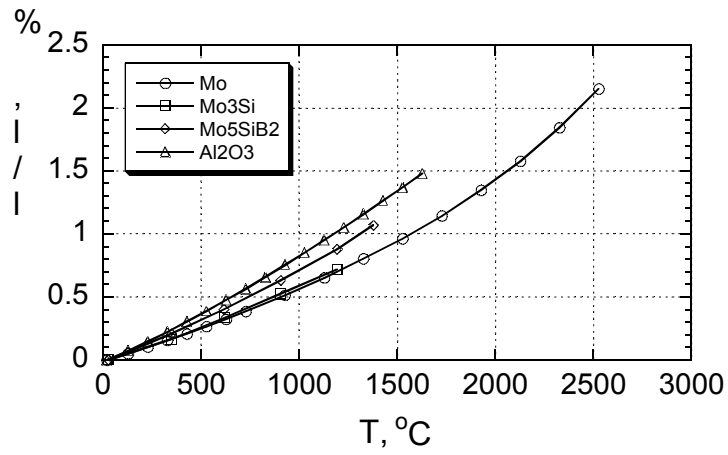


Fig. 5. Plot of thermal expansions,  $\Delta l/l$ , where  $\Delta l$  is the change in the initial specimen length  $l$ , as a function of temperature. The thermal expansion of alumina is higher than that of the phases in Mo-Si-B alloys.

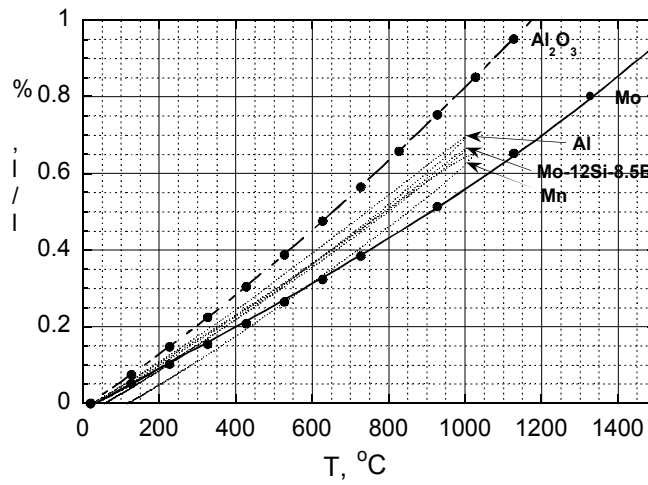


Fig. 6. Effect of alloying with Al or Mn on the thermal expansion of Mo-12Si-8.5B (at. %).

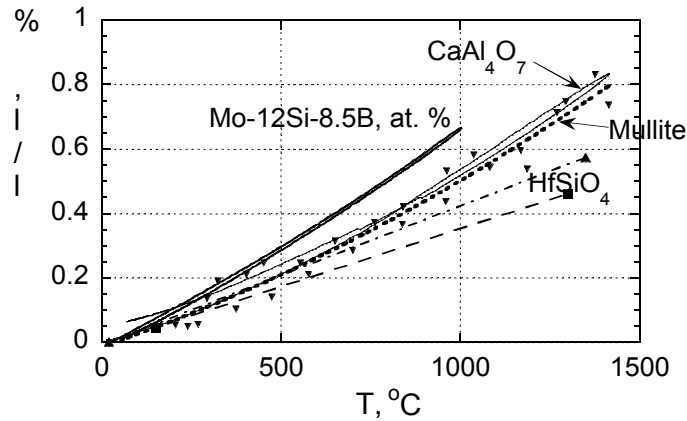


Fig. 7. Thermal expansion of potential coatings for Mo-12Si-8.5B (at. %).

### Microalloying with Zr

Alloys with different concentrations of Zr, substituting for Mo, were prepared by arc-melting followed by drop-casting and annealing in vacuum for 24 hours at 1600°C. The Zr additions did not change the microstructure significantly. The microstructures consisted essentially of Mo particles (bright) in a matrix of Mo<sub>3</sub>Si/Mo<sub>5</sub>SiB<sub>2</sub>, see Fig. 8. As the Zr concentration increased, the propensity for macrocracks in the cast and annealed ingots increased. The specimens with the higher Zr concentrations were therefore quite fragile. Figure 9 shows the trend in the room temperature fracture toughness when increasing amounts of Mo are substituted with Zr. More detailed data on the fracture toughness tests are listed in Table I. For some compositions several data points were collected in order to obtain an estimate for the scatter. It should be noted that the chevron-notch specimen technique employed here does not provide a rigorous value for the fracture toughness. However, it does reflect the trend in the fracture toughness values. Additions of Zr increased the room temperature fracture toughness noticeably. The maximum fracture toughness was found for Zr concentrations on the order of 2 at. %. The mechanism responsible for the toughening has not yet been identified, and the partitioning of the Zr in the three constituent phases of the alloy has not been measured. However, it is considered unlikely that the Zr additions would improve the fracture toughness of the brittle phases Mo<sub>3</sub>Si and Mo<sub>5</sub>SiB<sub>2</sub> with their complex crystal structures - it is more likely that the Zr improved the ductility/toughness of the  $\beta$ -Mo phase, as for example observed in TZM alloys.

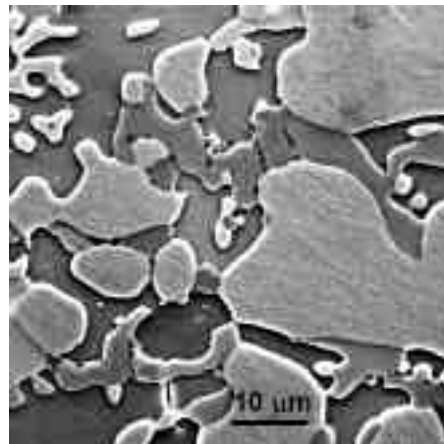


Fig. 8. SEM micrograph of etched Mo-1.5Zr-12Si-8.5B (at. %). The  $\beta$ -Mo appears as the bright particles.

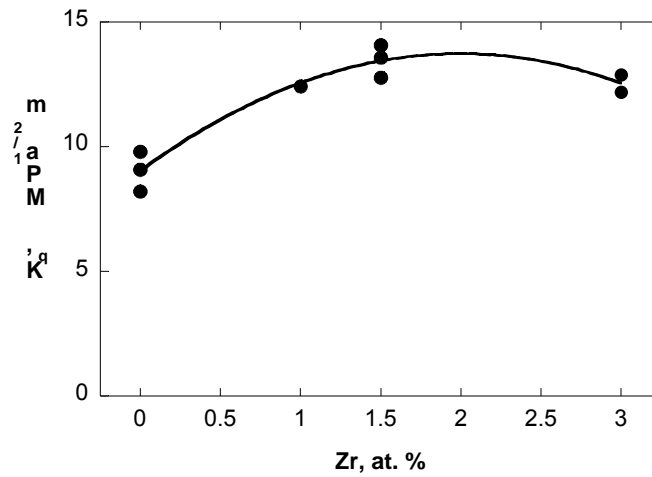


Fig. 9. Room temperature fracture toughness  $K_q$  of Mo-xZr-12Si-8.5B as a function of Zr concentration.

Table I. Fracture toughness  $K_q$  of Mo-Si-B alloys micro-alloyed with Ti or Zr.  $K_q$  was evaluated from Eqn. (1) assuming  $E=327$  GPa and  $\nu=0.29$ .

	Area of triangle broken during test, mm <sup>2</sup>	Absorbed energy, mJ	$G$ , J/m <sup>2</sup>	$K_q$ , MPa m <sup>1/2</sup>	$K_q$ , MPa m <sup>1/2</sup> , average±standard deviation
Mo-12Si-8.5B	2.94	0.68	231	9.1	
"	2.88	0.775	267	9.8	9.0±0.8
"	3.19	0.603	189	8.2	
Mo-12Si-8.5B-1Zr	2.82	1.09	432	12.4	
Mo-12Si-8.5B-1.5Zr	3.05	1.575	516	13.6	13.5±0.7
"	2.89	1.32	457	12.8	
"	3.48	1.93	555	14.1	
Mo-12Si-8.5B-3Zr	2.54	1.284	466	12.9	12.6±0.5
"	2.76	1.149	416	12.2	

### Ductilization with Spinel Particles

In the 1960's, Scruggs found that powder-metallurgical Cr is ductilized by addition of MgO particles that transform into MgCr<sub>2</sub>O<sub>4</sub> spinel particles.<sup>17</sup> Under the Fossil Energy Materials Program, M. P. Brady verified this ductilizing effect.<sup>18</sup> He determined that segregation of detrimental impurities such as nitrogen to the particle-matrix interface is one of the factors responsible for ductilization. Scruggs suggested that not only Cr, but also Mo can be ductilized by adding spinel particles.<sup>7</sup> In a preliminary experiment, nominally pure Mo and Mo-9 vol.% MgAl<sub>2</sub>O<sub>4</sub> coupons were prepared by hot-pressing at 1800°C. Figure 10 compares bend bars after room temperature testing and suggests that the spinel ductilization mechanism does occur.

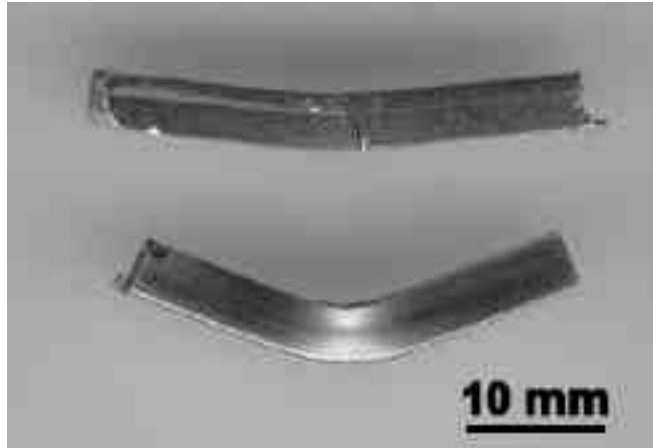


Figure 10. Qualitative comparison of the room temperature bend ductility of Mo (top) and Mo-9vol.% MgAl<sub>2</sub>O<sub>4</sub> (bottom).

Although this initial experiment seemed convincing, further work carried out to substantiate this effect has so far not been conclusive. A set of specimens of nominally pure Mo and Mo containing 5, 10, and 15 vol.% of MgAl<sub>2</sub>O<sub>4</sub> was hot-pressed (4h/1800°C/21 MPa). However, all these specimens were quite brittle. A combination of optical microscopy, SEM-EDS and x-ray diffraction showed that these materials contained significant amounts of MoO<sub>2</sub> inclusions. Near the edges of the coupons, i.e., close to the graphite hot-pressing dies, the MoO<sub>2</sub> was reduced to Mo and molybdenum carbide formed instead. It is concluded that the starting Mo powder was contaminated with oxygen. Another set of specimens was prepared with Mo powder obtained from a different source. Figure 11 shows the room temperature ductility of those specimens as a function of spinel volume fraction and strain rate. Significant scatter is observed, in particular for the “pure” Mo. Its ductility, at a strain rate of 10<sup>-4</sup> s<sup>-1</sup>, ranges from 11 to 52%. Figure 12 shows SEM micrographs of fracture surfaces of Mo. It is obvious that less ductile specimens fractured primarily along the grain boundaries, whereas more ductile specimens fractured transgranularly. Figure 13a shows the fracture surface of Mo-5 vol.% MgAl<sub>2</sub>O<sub>4</sub> to be a 50/50 mixture of intergranular and transgranular fracture; Fig. 13b is a lower magnification micrograph illustrating the presence of large (50 μm) spinel particles.

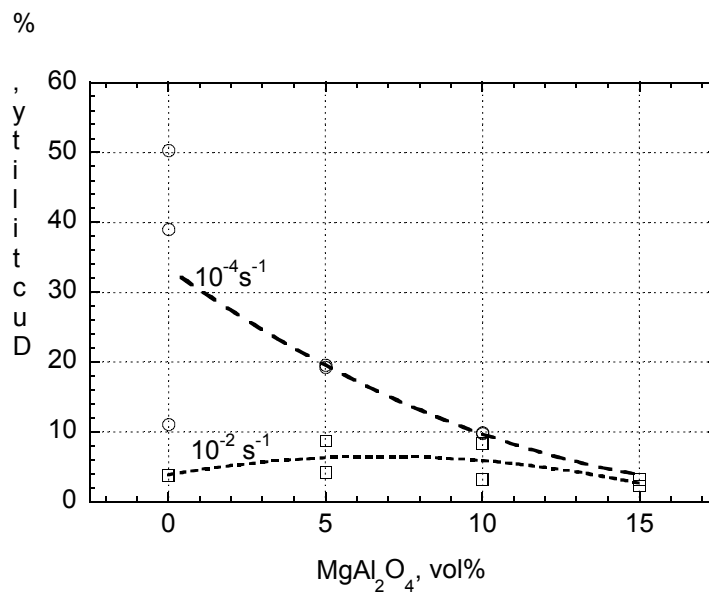
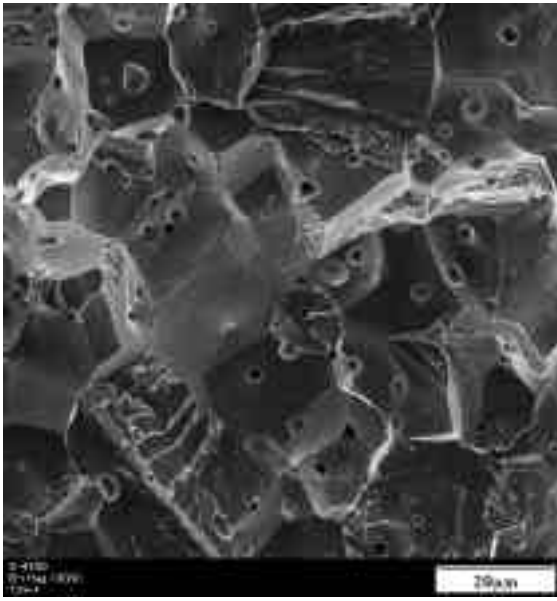
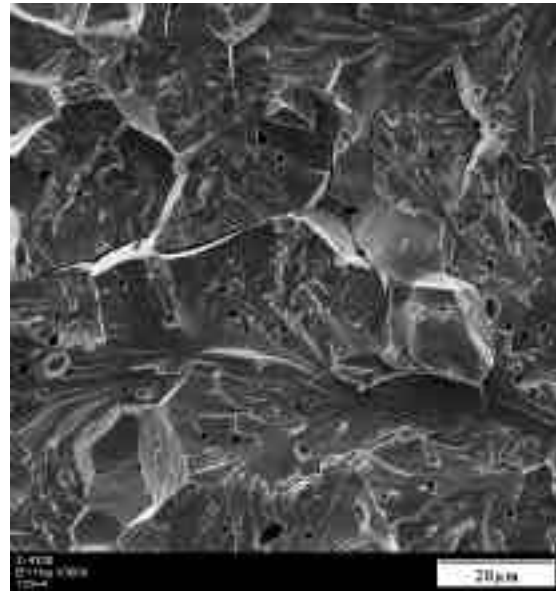


Fig. 11. Room temperature ductility as a function of MgAl<sub>2</sub>O<sub>4</sub> volume fraction and strain rate

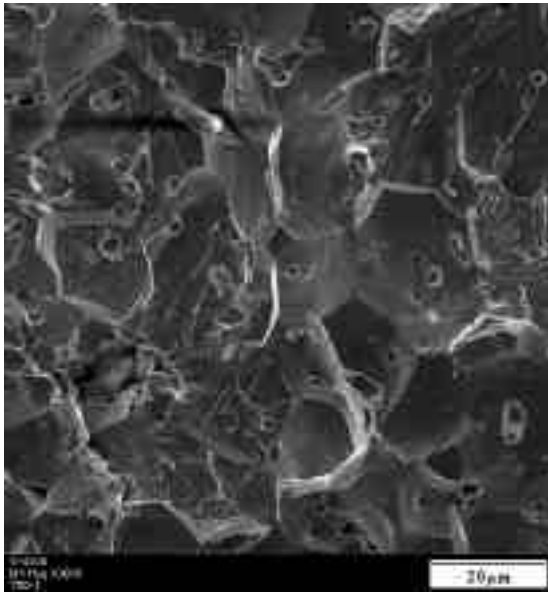


(a)

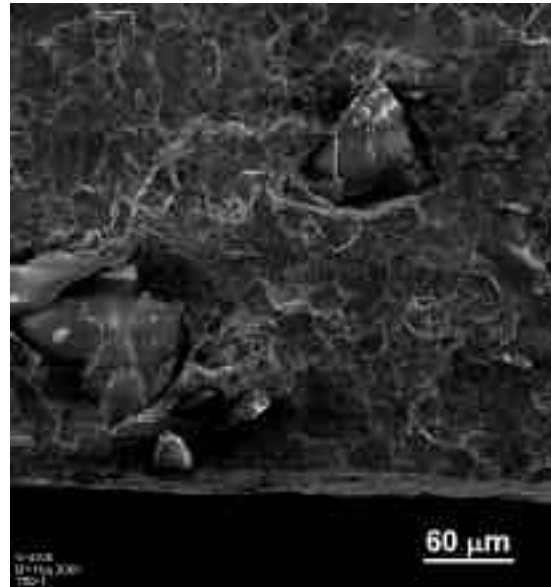


(b)

Fig. 12. SEM micrographs of fracture surfaces of two Mo specimens from the same hot-pressed disc tested at room temperature and  $10^{-4} \text{ s}^{-1}$ . One specimen (a) exhibited a ductility of 11%, whereas another (b) exhibited a ductility of 52%.



(a)



(b)

Fig. 13. SEM micrographs of room temperature fracture surfaces of Mo-5 vol.%  $\text{MgAl}_2\text{O}_4$  at different magnifications. The initial strain rate was  $10^{-4} \text{ s}^{-1}$ .

All the specimens were machined parallel to the hot-pressed discs. Because of interaction with the graphite die it is conceivable that the carbon concentration near the top and bottom of the discs is higher than that in the middle. According to Wadsworth, Nieh and Stephens<sup>19</sup> the C/O ratio is an important factor controlling the ductility of nominally pure Mo. Substantial room temperature ductility is only observed for atomic C/O ratios in excess of two. For values below two, intergranular fracture becomes important and the ductility decreases. Since we did not track the location of the specimens machined from the hot-pressed discs, their C concentration, and therefore their ductility, are likely to vary in a random manner.

Even though the results are inconclusive at this time, it is nonetheless surprising that the spinel-containing specimens are relatively ductile. The large  $\text{MgAl}_2\text{O}_4$  particles in Mo-5 vol.%  $\text{MgAl}_2\text{O}_4$  (Fig. 13b) would be expected to degrade the ductility substantially. However, this particular specimen did have a room temperature ductility of 20%. This suggests that a spinel ductilizing effect may exist, but more careful work is required to verify it. In future work, the C/O issue will be addressed. Also, it is imperative to quantify the fraction of transgranular and intergranular fracture. In particular, it is not clear whether the primary role of the spinel particles is to minimize the incidence of intergranular fracture, or whether spinel particles would ductilize a single crystal as well. Comparisons with “pure” Mo may be of doubtful value. Addition of even a small amount of  $\text{MgAl}_2\text{O}_4$  might change the residual impurity content and make therefore a comparison with “pure” Mo objectionable. A better strategy may be to determine whether there is a regime in which the ductility increases as the spinel volume fraction increases.

## REFERENCES

1. A. K. Vasudévan and J. Petrovic, “A comparative overview of molybdenum silicide composites,” *Mater. Sci. and Eng.* A155 (1992) 1-17.
2. D. M. Berczik, United States Patent 5,595,616 (1997), “Method for enhancing the oxidation resistance of a molybdenum alloy, and a method of making a molybdenum alloy.”
3. D. M. Berczik, United States Patent 5,693,156 (1997), “Oxidation resistant molybdenum alloys.”
4. T. A. Parthasarathy, M. G. Mendiratta, and D. M. Dimiduk, “Oxidation mechanisms in Mo-reinforced  $\text{Mo}_5\text{SiB}_2$  ( $\text{T}_2$ )  $\text{Mo}_3\text{Si}$  alloys,” *Acta Mater.* 50 (2002) 1857-1868.
5. V. Supatarawanich, D. R. Johnson, and C. T. Liu, “Effects of microstructure on the oxidation behavior of multiphase Mo-Si-B alloys,” *Mater. Sci. Eng.* A344 (2003) 328-339.
6. J. J. Kruzic, J. H. Schneibel, and R. O. Ritchie, “Fracture and Fatigue Resistance of Mo-Si-B Alloys for Ultrahigh-Temperature Structural Applications”, *Scripta Mater.* 50 (2004) 459-464.
7. D. M. Scruggs, “Ductile molybdenum composition containing a spinel dispersion,” United States Patent 3,320,036, Patented May 16, 1967.
8. J. H. Schneibel and E. d. Specht, “Slow crack growth in ternary B2 iron aluminides at room temperature,” *Scr. Metal. Mater.* 31 (1994) 1737-1742.
9. H. Choe, J. H. Schneibel, and R. O. Ritchie, “On the fracture and fatigue properties of Mo- $\text{Mo}_3\text{Si}$ - $\text{Mo}_5\text{SiB}_2$  refractory intermetallic alloys at ambient to elevated temperatures (25-1300°C),” *Metall. Mater. Trans.* 34A (2003) 25-239.
10. J. H. Schneibel, P. F. Tortorelli, M. J. Kramer, A. J. Thom, J. J. Kruzic, and R. O. Ritchie, “Optimization of Mo-Si-B Intermetallics,” in *Defect Properties and Related Phenomena in Intermetallic Alloys*, E. P. George, M. J. Mills, H. Inui, G. Eggeler, eds., MRS Symposium Proceedings, vol. 753, Materials Research Society, Warrendale, PA, 2003, BB2.2.1-6.
11. J. H. Schneibel, C. T. Liu, D. S. Easton, and C. A. Carmichael, “Microstructure and mechanical properties of Mo- $\text{Mo}_3\text{Si}$ - $\text{Mo}_5\text{SiB}_2$  silicides,” *Mater. Sci. Eng. A*, A261 (1999) 78-83.
12. J. H. Schneibel, D. S. Easton, H. Choe, and R. O. Ritchie, “Fracture Toughness, Creep Strength and Oxidation Resistance of Mo- $\text{Mo}_3\text{Si}$ - $\text{Mo}_5\text{SiB}_2$  Molybdenum Silicides,” in “Structural Intermetallics, Third International Symposium,” K. J. Hemker and D. M. Dimiduk, eds., TMS, Warrendale, PA, 2001, pp. 801-809.
13. A. Yu. Koval, A. D. Vasilev, and S. A. Firstov, “Fracture Toughness of Molybdenum Sheet under Brittle-Ductile Transition,” *Int. J. of Refractory Metals & Hard Materials*, 15 (1997) 223-226.
14. Y. S. Touloukian, R. K. Kirby, R. E. Taylor, and P. D. Desai, “Thermophysical Properties of Matter Vol. 12 (Thermal Expansion),” Purdue University, Lafayette, IN, 1975.
15. C. J. Rawn, J. H. Schneibel, C. M. Hoffmann, and C. R. Hubbard, “The crystal structure and thermal expansion of  $\text{Mo}_5\text{SiB}_2$ ,” *Intermetallics* 9 (2001) 209-216.
16. CINDAS LLC TPMD Database, [www.cindasdata.com](http://www.cindasdata.com)

17. D. M. Scruggs, L. H. Van Vlack, and W. M. Spurgeon, *J. Amer. Ceram.Soc.* 51 (1968) 473.
18. M. P. Brady, I. M. Anderson, M. L. Weaver, H. M. Meyer, L. R. Walker, M. K. Miller, D. J. Larson, I. G. Wright, V. K. Sikka, a. Rar, G. M. Pharr, J. R. Keiser, and C. A. Walls, "Nitrogen impurity gettering in oxide dispersion ductilized chromium," *Materials Science and Engineering A* 50 (2004) 459-464.
19. J. Wadsworth, T. G. Nieh, and J. J. Stephens, "Dilute Mo-Re alloys - a critical evaluation of their comparative mechanical properties," *Scr. Metall.* 20 (1986) 637-642.